JTTEE5 9:126-132

Elastic and Inelastic Effects in Compression in Plasma-Sprayed Ceramic Coatings

V. Harok and K. Neufuss

(Submitted 2 December 1999; in revised form 29 February 2000)

Four-point bend tests of a plasma-sprayed zircon ($ZrSiO_4$) coating are presented, the coating being prepared by atmospheric plasma spraying (APS) spraying onto a titanium alloy substrate, using a water-stabilized plasma (WSP) torch. The mechanical behavior in compression of the coating material is nonlinear, including hysteresis (9% of the maximum strain) and permanent deformation. The effective in-plane Young's modulus is about 13 GPa for very small strains and doubles for a compressive strain of –0.18%. Possible micromechanisms to explain this behavior are proposed, and some general protocols concerning the testing of plasma-sprayed ceramic coatings are deduced.

Keywords elastic modulus, mechanical properties, micromechanism of deformation, and zircon coating

1. Introduction

In the process of plasma spraying, materials are produced whose properties differ substantially from the bulk; the difference is induced by their unique microstructure.

For plasma-sprayed ceramic coatings, successive spray passes create a lamellar microstructure[1] with micro areas of imperfect adhesion between lamellae. In the course of processing, high *residual stresses* are generated in the material: *primary* or *quenching* stresses as a result of intense cooling of splats subsequent to solidification and *secondary* stresses as a result of different thermal expansion coefficients of the coating and of the substrate. The residual stresses relax partially by the formation of numerous microcracks perpendicular to the coating plane.

This material is generally as follows:

- *microscopically inhomogenous*, (Ref 1, p. 155), since different phases are formed within the coating (*e.g.*, Ref 8). Also, microscopic defects such as microcracks and roughly spherical pores may be considered as inhomogeneities.
- *macroscopically inhomogenous*, since there is a gradient of properties across the coating thickness. The cooling rate is higher for splats close to the metallic substrate than for splats on the surface of a thick ceramic coating (Ref 1, Section 6.2). Thus, the phase composition, residual stresses, and microcracking may be different.
- *anisotropic*, since the material properties are different in the spraying direction and in the deposition plane (*i.e.*, transverse isotropy). The elastic behavior is, therefore, completely described by five independent elastic constants.[2]

V. Harok and **K. Neufuss,** Institute of Plasma Physics, 182 21 Praha 8, Czech Republic. (Mr. Harok has since left the Institute of Plasma Physics, and can now be contacted at Bontaz Centre CZ, V. Noveho 973, 33701 Rokycany, Czech Republic.) Contact e-mail: neufuss@ipp.cas.cz.

If the strains are so small that macroscopic damage does not appear, the mechanical behavior is frequently called *elastic* behavior because ceramics generally exhibit no plasticity at room temperature. Although inelastic effects are rarely analyzed in experimental studies on ceramic coatings, a form of *pseudoplastic* behavior at room temperature is mentioned in Ref 1 (p. 246).

The effective Young's modulus of plasma-sprayed ceramics is much lower than that of the bulk due to microcracks and pores.[1,2] Kroupa and Dubsky[3] have predicted an *increase of the modulus* with increasing compressive strain, due to successive complete closing of microcracks, by analogy to the elastic behavior of rocks. Numerous studies in the field of geomechanics[4,5] could be extended to plasma-sprayed ceramics.

2. Test Specimen

The test specimen was prepared by atmospheric plasma spraying of zircon ($ZrSiO_4$) powder onto a grit-blasted titanium alloy substrate. Zircon plasma-sprayed coatings[6] are industrially used in thermal and diffusion barriers as an inexpensive substitute of ZrO_2 for less sophisticated applications. The deposits prepared by plasma spraying of zircon are composed of tetragonal ZrO_2, monoclinic ZrO_2, and glassy SiO_2 phases.[7,8] Selected properties of the bulk materials are presented in Table 1.

The substrate material was T110 wrought titanium alloy,[10] whose properties (Table 2) and applications are similar to Ti-6Al-4V alloy.[11,12] The choice of the substrate material was made with respect to its high maximum elastic strain and low elastic stiffness, to increase the accuracy of the measurements. The material was machined to the dimensions given in Table 3. The substrate surface was grit blasted with 0.6 mm alumina grit.

Zircon powder was sprayed with a water-stabilized plasma torch PAL 160. The characteristics of this plasma torch are presented in Table 4; the feeding powder characteristics and spray process parameters are presented in Table 5; and the final coating thickness is presented in Table 3. The thickness of the coating and of the substrate were measured with a mechanical micrometer at 12 points. The spray process was controlled with the assistance of a thermocouple situated on the back side of the

Table 1 Selected bulk properties of the feeding powder material ($ZrSiO_4$) and of the phases present in the deposit[6,7,9] (t—tetragonal, and a—amorphous)

$ZrSiO_4$ softening point	2015 °C
$ZrSiO_4$ phase decomposition temperature	1676 °C
$ZrSiO_4$ density	4600 kg m^{-3}
t-ZrO_2 Young's modulus	10 GPa
t-ZrO_2 Coefficient of linear thermal expansion	7.1×10^{-6} K^{-1}
a-SiO_2 Young's modulus	75 GPa
a-SiO_2 Coefficient of linear thermal expansion	0.5×10^{-6} K^{-1}

Table 2 Basic properties of the substrate material[10,12]

Specification	T110 alloy
Chemical composition	Base Ti, 6% Al, 3% Mo, 2% Cr
Young's modulus	110 GPa
Yield stress	$R_{p0.2} \approx 800$ MPa
Maximum elastic strain	≈0.7%
Coefficient of linear thermal expansion	11×10^{-6} K^{-1}

Table 3 Specimen dimensions

Specimen length		118 ± 0.5	mm
Specimen width	*B*	19.4 ± 0.1	mm
Substrate thickness	*H*	2.59 ± 0.02	mm
Coating thickness	*h*	1.69 ± 0.04	mm

Table 4 Basic parameters of the plasma torch[13]

Specification, supplier	PAL 160, IPP Prague
Work medium	H_2O
Arc current/voltage	490 A/305 V
Plasma mass flow rate	0.29 g s^{-1}
Centerline density	0.98 g m^{-3}
Centerline temperature	26,000 K
Centerline velocity	5600 ms^{-1}

Table 5 Basic feeding powder characteristics and plasma spray process parameters

Feeding powder composition	$ZrSiO_4$
Feeding powder size	40-70 μm
Process: plasma torch	APS; PAL 160
Feeding rate	24 kg h^{-1}
Preheating	120 °C
Number of spraying cycles	20
Feeding/spraying distance from the exit nozzle	25 mm/365 mm

substrate. Initial preheating of the substrate with a plasma jet was followed by 20 spray cycles (Fig. 1).

3. Experimental Setup

An Instron 1362 (Canton, MA) electromechanical testing machine was used, equipped with a 1 kN load cell, a four-point bend test fixture, and a deflection gauge (Fig. 2). The system was designed to provide high accuracy in testing of substrate-coating plate or beam specimens.

Parameters of the fully articulating four-point bend test fixture[14] are presented in Table 6. The loading arm is swinging in

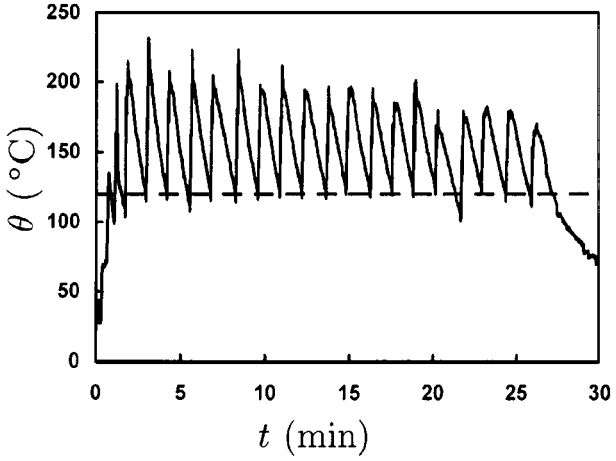

Fig. 1 Record of the substrate temperature in the course of spraying

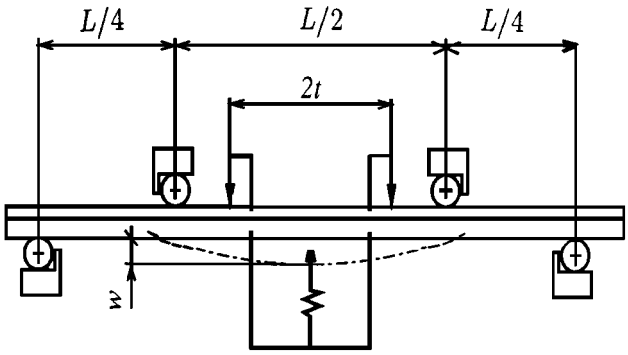

Fig. 2 Test configuration

Table 6 Parameters of the four-point bend test fixture and of the deflexion gauge

Fixture support span	*L*	94.0 ± 0.2	mm
Fixture loading span	*L*/2	47.0 ± 0.1	mm
Fixture bearing cylinder diameter		5.0 ± 0.0	mm
Deflexion gauge hangers span	2*t*	32.0 ± 0.5	mm

the figure plane, to uniformly distribute the loading force. Three of the four supports swing around the axes parallel to the specimen axis to avoid torsion of the specimen. Hardened steel cylindrical bearings are used.

The deflection gauge consists of two hangers and an Instron strain-gauge displacement sensor, Catalog No. 2620-603. It is hung on the tested specimen, independently of the fixture (Fig. 2). For small deflexions *w*, the curvature 1/*R* of the specimen is given by

$$\frac{1}{R} = \frac{2}{t^2} w \qquad \text{(Eq 1)}$$

where 2*t* represent the hanger span (Table 6). The deflection gauge was calibrated by the insertion of a small plate standard between the displacement sensor and the testing specimen. The thickness of the standard was (0.250 ± 0.005) mm. The calibration was checked after testing.

Table of Symbols	
$\overline{\varepsilon_l}$	mean longitudinal strain in the coating (1)
$\underline{\varepsilon_l}$	longitudinal strain at the substrate-coating interface (1)
η	strain biaxility factor (1)
υ	substrate Poisson's ratio (1)
$\overline{\sigma_l}$	mean longitudinal stress in the coating (Pa)
τ_{12}	shear stress in the deposition plane (Pa)
$2a$	microcrack length (m)
B	specimen width (m)
$2b$	microcrack opening displacement (m)
C	slope of the load-deflection curve (N m^{-1})
C^{sec}	secant stiffness of the specimen (N m^{-1})
E	substrate Young's modulus (Pa)
E^*	effective substrate Young's modulus (Pa)
E_r	effective in-plane Young's modulus of the coating (Pa)
$E^{sec}{}_r$	effective secant "modulus" of the coating (Pa)
F	loading force (N)
F_{av}	average loading force in a hysteresis loop (N)
H	substrate thickness (m)
h	coating thickness (m)
K	flexural stiffness of the specimen (N m^2)
R	radius of curvature (m)
$R_{p0.2}$	substrate yield point (Pa)
$2t$	deflection gauge hangers span (m)
w	deflection (m)
z_0	position of the neutral axis (m)

Table 7 Mechanical sensors. Specifications after Instron

Specification	Load cell	Displacement sensor
Catalogue no.	2518-204	2620-603
Static range	±1 kN	±1 mm
Repeatability	0.2%(a)	0.05%(b)
Linearity	±0.4%(a)	–0.07%(b)
Hysteresis	0.2%(a)	–0.05%(b)

(a) Maximum error in percent of reading
(b) Error in percent of full scale displacement

In the four-point bend test fixtures, the bending moment is generated with a total error less than 1.5%. Maximum errors of the load cell are presented in Table 7. The individual errors of the deflection gauge are given by the repeatability of the displacement sensor (Table 7). The total error of the determination of $1/R$ is 3%. This error arises mostly by the error of the hangers span $2t$ and by the error of the calibration.

The crosshead speed was set to 0.060 mm min^{-1}, which corresponds to the strain rate of 3×10^{-6} s^{-1} within the coating. Loading programs are detailed in Section 6.

4. Application of the Elasticity Theory

Deformation in four-point bending of the coating-substrate specimen is cylindrical between the inner (loading) supports.

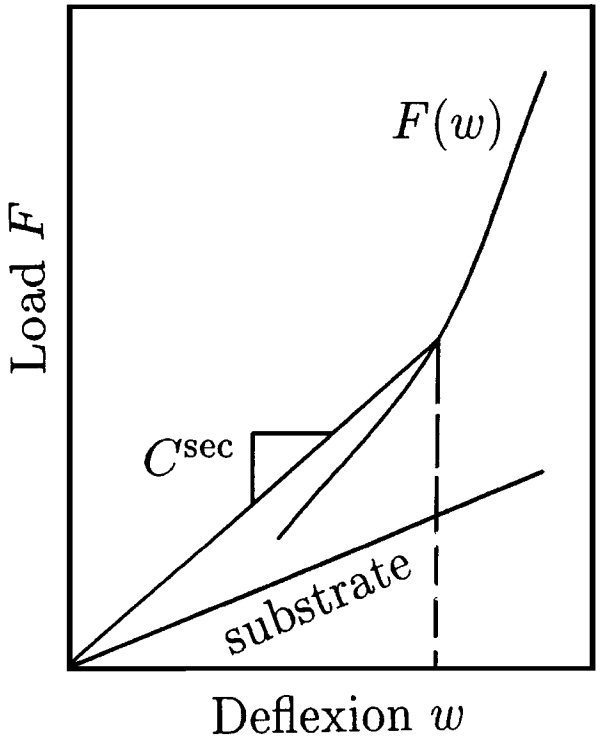

Fig. 3 Evaluation of the load-deflection curves in the case of nonlinear behavior of the coating

For *linear elastic* materials of the coating and of the substrate, the curvature $1/R$ of the specimen loaded by force F is given by

$$\frac{1}{R} = \frac{FL/8}{K} \qquad \text{(Eq 2)}$$

where $L/2$ and L represent the loading and the support span, respectively. Constant K is given[15] by the thickness of the substrate H, thickness of the coating h, width of the specimen B, and by material constants E_r (coating), E, and v (substrate):

$$K = \frac{E_r^2 h^4 + E^{*2} H^4 + 2E_r E^* hH\left(2h^2 + 2H^2 + 3hH\right)}{12(hE_r + HE^*)} B \qquad \text{(Eq 3)}$$

In the equation, $E^* = \eta E$, where E is the Young's modulus of the substrate and η is a constant; the value of η lies between 1 and $1/(1 - v^2)$, for $H << B$ (plane stress) or $H >> B$ (plane strain), respectively. The term E_r represents the effective in-plane Young's modulus of the coating. Taking into account the experimental errors, distinction of the coating stiffness under the conditions of the plane stress/plane strain is of only limited interest; and therefore, E_r is used in Eq 3.

The load-deflection curve for linear elastic behavior is represented by a line with slope $C = dF/dw$:

$$C = \frac{16}{Lt^2} K \qquad \text{(Eq 4)}$$

Position z_0 of the neutral axis is

$$z_0 = \frac{H^2 E^* - h^2 E_r}{2(HE^* - hE_r)} \qquad \text{(Eq 5)}$$

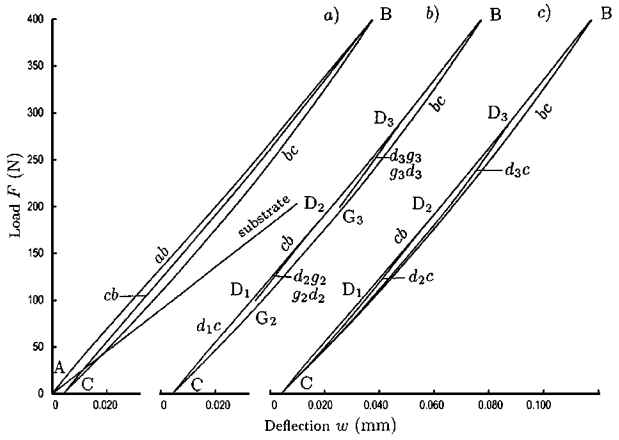

Fig. 4 Load-deflection curves measured in four-point 1bending: (**a**) first four loading cycles, (**b**) partial unloading program, and (**c**) partial hysteresis curves. In part (a), the loading curve for the substrate without coating is added

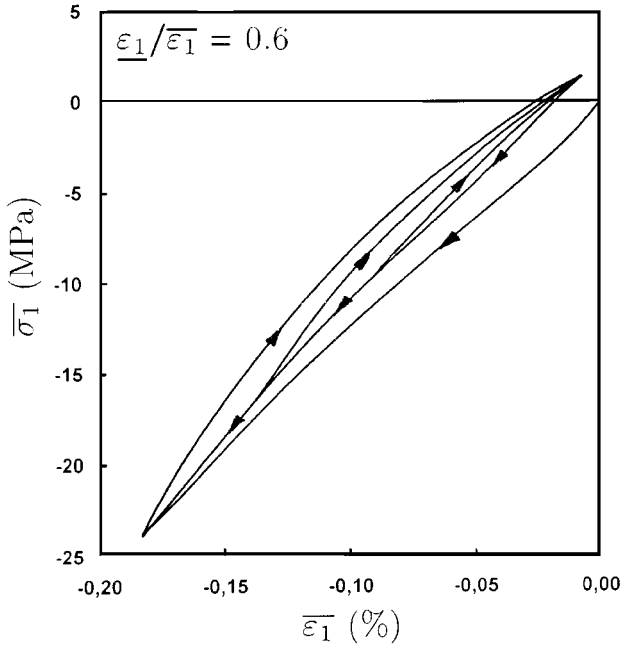

Fig. 5 Mean coating stress-mean strain curves for the coating material

from the substrate-coating interface. The longitudinal strain at the substrate-coating interface $\underline{\varepsilon_1}$ and the mean longitudinal strain in the coating $\overline{\varepsilon_1}$ are

$$\underline{\varepsilon_1} = \frac{2}{t^2} z_0 \, w \quad \text{and} \quad \overline{\varepsilon_1} = \frac{2}{t^2}\left(z_0 + \frac{h}{2}\right) w \qquad \text{(Eq 6)}$$

Consider now a *nonlinear behavior of the coating* E_r $(\overline{\varepsilon_1})$ on the linear elastic substrate E, resulting in a nonlinear load-deflexion curve $F(w)$. In Fig. 3, a curve $F(w)$ is displayed together with the load-deflection curve for the substrate without the coating. At a given deflection w, the mean longitudinal stress in the coating $\overline{\sigma_1}$ must be the same as if the coating material were linear elastic, with a Young's modulus $E^{sec}{}_r(w)$, which is given by Eq 3 and 4 for $C^{sec}(w) = F(w)/w$. The position of the neutral axis $z_0(w)$ may, therefore, be calculated from Eq 5, substituting $E^{sec}{}_r(w)$ for E_r. Function $z_0(w)$ may be substituted for z_0 in Eq 6 to obtain $\overline{\varepsilon_1}(w)$ and finally

$$\overline{\sigma_1}(w) = E_r^{sec}(\omega)\,\overline{\varepsilon_1}(w) \qquad \text{(Eq 7)}$$

The coating mean stress-mean strain curves $\overline{\sigma_1}(\overline{\varepsilon_1})$ are determined by $\overline{\sigma_1}(w)$ together with $\overline{\varepsilon_1}(w)$. In this way, experimental load-deflection curves of the substrate-coating specimen are transformed into the proper coating characteristics.

5. Reference Test

A reference four-point bend test was made on the substrate, before grit blasting. The experimental load-deflection curve was highly linear (nonlinearity lower than 0.3%), and the hysteresis was lower than 0.04% of the maximum load of 291 N. Maximum deflexion was 0.123 mm. The resulting modulus E^* of the substrate was $E^* = (114 \pm 6)$ GPa.

6. Experimental Results

Experimental *load-deflection curves* of the substrate-coating specimen are presented in Fig. 4. The coating was on the compression side of the specimen.

Figure 4a shows where the test specimen was loaded to 400 N (from A to B *via ab*), then unloaded to zero force (to C *via bc*), reloaded (to B *via cb*), and unloaded again (*via bc*). Then, two other loading cycles were performed; the loading and unloading curves were still *cb* and *bc*, respectively.

After the first four simple loading cycles, the loading according to Fig. 4(b) was performed; loading to 100 N (from C to D_1 *via cb*), unloading to zero force (from D_1 to C *via* d_1c, which coincide with *cb* in the figure), loading to 200 N (from C to D_2 *via cb*), unloading to 100 N (to G_2 *via* d_2g_2), loading to 300 N (from G_2 to D_3 *via* g_2d_2 and *cb*), unloading to 200 N (from D_3 to G_3 *via* d_3g_3), loading to 400 N (from G_3 to B *via* g_3d_3 and *cb*), and finally unloading (from B to C *via bc*).

In Fig. 4(c), the specimen was loaded to 100 N (from C to D_1 *via cb*), unloaded to zero force (from D_1 to C *via* d_1c). Then, it was loaded to 200 N (from C to D_2 *via cb*), unloaded to zero force (to C *via* d_2c), loaded to 300 N (from C to D_3 *via cb*), unloaded to zero force (to C *via* d_3c), loaded to 400 N (from C to D_3 *via cb*), and finally unloaded (from B to C *via bc*).

The coating material can not be described as linear elastic for the following two reasons.

1. *Inelastic effects*: The deformation of the testing specimen is generally dependent on the loading path. This effect is generated by the coating (the substrate is linear elastic, as discussed in Section 8) and it is similar to the cyclic plasticity of metals, as follows.

a. *Initial loading curve*. When initially loaded, the loading curve is different from that of the next loading.

b. *Hysteresis loop*. For cyclic loading, the loading and unloading curves form a stationary hysteresis loop, determined by the maximum-minimum load.

c. *Permanent deformation*. The permanent deformation of the specimen is given by the position of point C in Fig. 4(a).

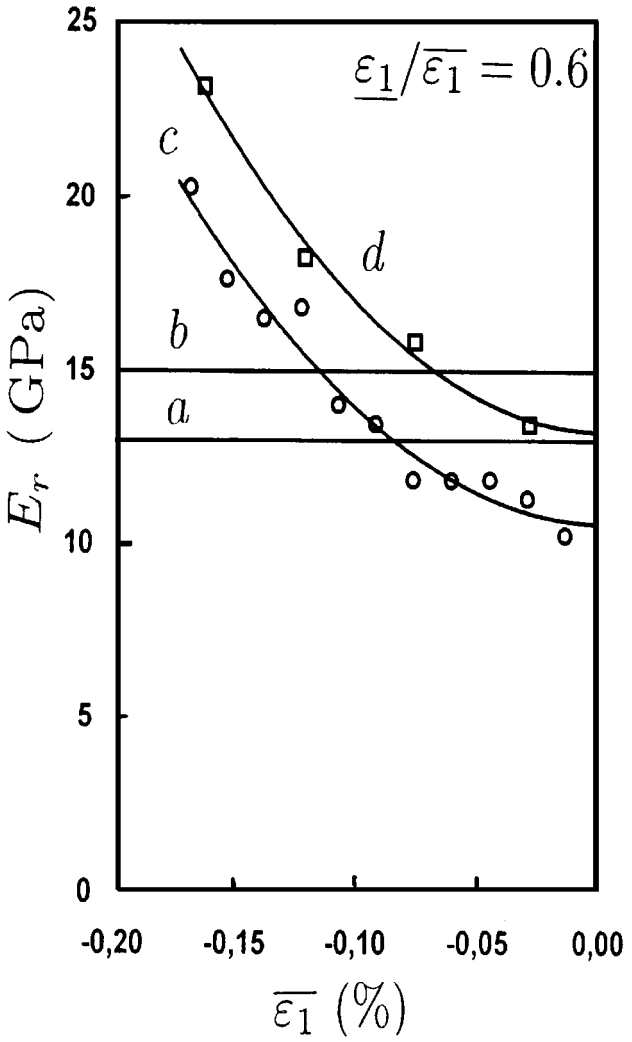

Fig. 6 Effective in-plane Young's modulus of the coating material calculated by different methods: (**a**) secant modulus (from points AB), (**b**) secant modulus (from points CB), (**c**) average curve, and (**d**) partial unloading

d. *Deformation-induced residual stresses*. The permanent deformation of the coating should result in additional residual stresses in the coating and in the substrate after unloading. If the coating has been loaded in compression, the deformation-induced residual stress is tensile in the coating. These residual stresses contribute to the residual stresses already present in the coating.

2. *Elastic nonlinearity*. Neglecting inelastic effects, the load-deflection curve is still nonlinear.

To obtain quantitative results concerning the coating material, the load-deflection curves were transformed into *stress-strain curves*. The evaluation was made in terms of the mean longitudinal coating stress $\overline{\sigma_1}$ and the mean longitudinal coating strain $\overline{\varepsilon_1}$ according to Section 4. The resulting curves for Fig. 4(a) and (c) are presented in Fig. 5. The maximum load corresponds to a mean strain of –0.183% and to the mean stress of –23.9 MPa. The permanent strain is –0.008%; the deformation-induced residual stress is 1.5 MPa. The hysteresis represents 9% of the maximum compressive strain. Globally, the stiffness of the coating material increases with the compressive strain.

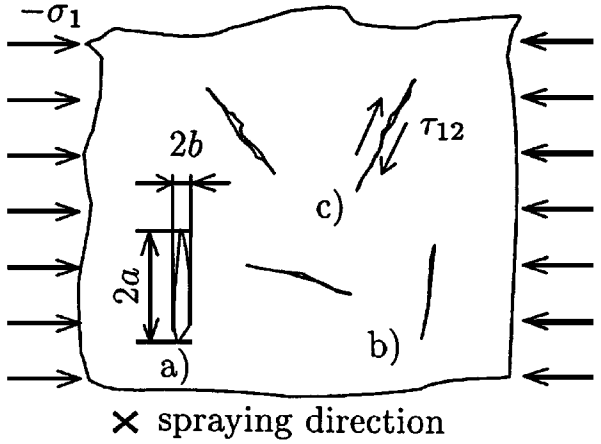

Fig. 7 Effect of microcracks on the mechanical behavior of plasma-sprayed coatings

7. Effective In-plane Young's Modulus

Although the Young's modulus has been defined for purely elastic materials, various approaches are used in technical praxis to obtain its effective value in the case of the presented inelastic behavior. Four examples are presented in Fig. 6:

1. *The secant modulus for the initial load-deflexion curve*. Taking the slope of the line AB (Fig. 4) as C in Eq 4, we obtain, from Eq 5 and 6, the value of E_r = 13 GPa. The strain range should be presented together with the value of the modulus.

2. *The secant modulus for the hysteresis loop*. Taking the slope of the line CB (Fig. 4) as C in Eq. 4, we obtain, from Eq 5 and 6, the value of E_r = 15 GPa. The strain range should be presented together with the value of the modulus.

3. *Average of the two branches of the hysteresis loop*. The modulus $E_r(w)$ is calculated from Eq 4 to 6 by the substitution $C = dF_{av}/dw$, where $F_{av}(w)$ represents the average of the actual load in loading and unloading branches. The function $E_r(w)$ is transformed to $E_r(\overline{\varepsilon_1})$. The modulus increases from 10 GPa at the mean strain – 0.008% to 20 GPa at the mean strain –0.183%.

4. *Method of partial unloading*. In Fig. 4, partial unloading curves are represented by lines d_ig_i. The mean modulus E_r is determined from Eq 4 to 6 by substitution $C = C_i$, where C_i are slopes of the unloading curves on particular intervals of w. Resulting $E_r(\overline{\varepsilon_1})$ increases from 13 GPa at the mean strain of – 0.008% to 25 GPa at the mean strain of – 0.183%.

The estimated total experimental error of E_r is ± 2 GPa, which represents 8 to 18% of its value.

8. Confirmation Tests

Two additional four-point bend tests were carried out on an as-machined substrate and on the same specimen after grit blasting, to detect a possible influence of grit blasting on the experimental results. The material, the specimen dimensions, the

experimental conditions, and the loading programs were identical with those in Sections 2, 3, and 6. In both cases, the load-deflection curves were linear (nonlinearity better than 0.4%) and the hysteresis was negligible (less than 0.2%). The difference between the slopes of particular lines was less than 1%. The nonlinearity and inelastic effects observed on the substrate-coating specimen, therefore, are generated *exclusively by the coating*.

9. Discussion

The sensitivity and accuracy of the experimental setup allowed at the detection and quantification of the phenomena that are unexplored experimentally and only incompletely explained theoretically in plasma-sprayed coatings.

As a result of the presence of microcracks,[2] the experimental values of the effective in-plane Young's modulus of the coating (11 to 25 GPa) are small compared to bulk material (on the order of 100 GPa, Table 1). This fact is well known in plasma-sprayed materials although it is frequently presented rather in relation with the total porosity (Ref. 1, p. 185) than with the microcracks (the microcracks contribute slightly to the total porosity[2]).

The *increase of the effective in-plane Young's modulus* of the coating in compression has been predicted as a pure elastic effect in Ref 3; *i.e.*, the microcracks orientated perpendicularly to the principal stress (Fig. 7 a and b) close in compression. The closing stress is proportional to the ratio b/a. As there is a great number of microcracks with different b/a within the material, the effective Young's modulus increases with the compressive strain. This experimental study represents direct proof of this phenomenon.

The *inelastic effects* including the permanent deformation and hysteresis have not been generally considered to take place in plasma-sprayed ceramics. We suppose that the phenomena are caused by internal friction, by analogy to the behavior of rocks.[5] Thus, consider a microcrack orientated as in Fig 7(c). Shear stresses are generated on its faces, causing relative displacements along the microcrack plane. Frictional forces between the faces of such microcracks result in macroscopic hysteresis and permanent deformation. The inelastic effects are observed in rocks under uniaxial compression.[5] Under hydrostatic pressure,[4] pure elastic behavior is observed in rocks because there is no shear stress present within the material.

We have also observed the same type of behavior (including nonlinearity and inelastic effects) in other plasma-sprayed ceramics, *e.g.*, in various alumina coatings.

Regarding the method of evaluation of the test results, the method of partial unloading (item 4 in Section 7) seems to represent the best method to determine the effective Young's modulus of the coating. If decreasing the amplitude of unloading, the values of the modulus should get near to those obtained by the ultrasonic method, under the compressive prestress (by analogy to Ref. 5).

The evaluation was made in terms of mean values (mean stress and mean strain) across the coating thickness. One consequence is that possible macroscopic inhomogeneity (Section 1) of the material is neglected. Another consequence is that the curve representing the strain dependence of the effective in-plane Young's modulus is "smoothed." The difference between local and mean values of longitudinal strain is proportional to the coating thickness. Thus, the most correct material characteristics would have been obtained theoretically for a thin coating $(\varepsilon_1 / \overline{\varepsilon_1} \approx 1)$. In this case, the experimental errors would increase drastically; a compromise on the coating thickness should therefore be found.

It should be pointed out that nonlinearity and hysteresis may be expected also for *tensile* loading of the coating, due to the growth of the microcracks and their interconnection into macroscopic cracks. This completely different effect is not studied in this paper.

10. Conclusions

The mechanical behavior in compression of plasma-sprayed ceramics may be generally considered nonlinear and inelastic.

Considering the presence of the inelastic effects, a special approach in preparation of test specimens, in the test design, and in the evaluation is necessary. Test specimens should be carefully prepared, transported, and stored to avoid deformation of the coating. The loading history of the specimen should be recorded, since the material has its "memory" represented by permanent deformation and residual stresses.

The evaluation method should always be specified. Values of the effective Young's modulus may differ considerably for the same test and specimen using different evaluation methods. Without the elimination of the inelastic effects, measured values of the Young's modulus may depend on the experimental technique, and, in many cases, they do (Ref 1, p. 241). The method of partial unloading, presented in the paper, should give values of the Young's modulus comparable to ultrasonic tests.

A complex model of the mechanical behavior including inelastic effects is necessary to (1) define the Young's modulus on physical basis and (2) quantify the inelastic effects.

Mechanical testing of plasma-sprayed coatings prepared under different conditions allows the relation between the spray process parameters, microstructure, residual stresses, and properties of these materials to be understood.

Acknowledgments

The authors thank P. Jaros, for invaluable consultations on the experimental setup, and J. Siegel, H. Lauschmann, J. Dubsky, K. Volenik, and J. Matejicek, for assistance and helpful discussions. Special thanks are dedicated to F. Kroupa, for critical comments on the manuscript. The project has been partially supported by Grants GACR Nos. 106/97/S008 and 106/97/0775.

References

1. L. Pawlowski: *The Science and Engineering of Thermal Sprayed Coatings*, John Wiley, Chichester, 1995.
2. F. Kroupa, and M. Kachanov: *Proc. 19th Riso Int. Symp.*, J.V. Carstensen, T. Leffers, T. Lorentzen, O.B. Pedersen, B.F. Sorensen, G. Winther, eds., Riso National Laboratory, Roskilde, 1998, pp. 325-30.
3. F. Kroupa and J. Dubsky: *Scripta Mater.*, 1999, vol 40 (11), pp. 1249-54.

4. J.B. Walsh: *J. Geophys. Res.*, 1965, vol. 70 (2), pp. 381-389.
5. J.B. Walsh: *J. Geophys. Res.*, 1965, vol. 70 (2), pp. 399-411.
6. P. Chraska, K. Neufuss, and H. Herman: *J. Thermal Spray Technol.*, 1997, vol. 6 (4), pp. 445-48.
7. A. Rudajevova: *Surface Coating Technol.*, 1994, No. 64, pp. 47-51.
8. J. Dubsky, K. Neufuss, and B. Kolman: *Thermal Spray: A United Forum for Scientific and Technological Advances*, C. C. Berndt, ed., ASM International, Materials Park, OH, 1997, pp. 473-76.
9. T. Allen, J. Cotton, P. Dragun, R. James, A. Marsh, M. Ori, B. Pace, B. Swindells: *The Technical Ceramics Handbook*, Wade Advanced Ceramics Ltd., Burslem, Stoke-on-Trent, United Kingdom, 1993.
10. Anon.: TPC 204-140/71, SONP Kladno, Czech Republic, 1971 (in Czech).
11. J.D. Destefani: *Metals Handbook*, 10th ed., C.T. Liu, J.O. Stiegler, and F.H. Froes, eds., ASM International, Materials Park, OH, 1990, vol. 2, pp. 586-91.
12. S. Lampman: *Metals Handbook*, 10th ed., C.T. Liu, J.O. Stiegler, and F.H. Froes, eds., ASM International, Materials Park, OH, 1990, vol. 2, pp. 592-633.
13. M. Hrabovsky, M. Konrad, V. Kopecky, and V. Sember: *IEEE Trans. Plasma Sci.*, 1997, vol. 25 (5), pp. 833-939.
14. Anon.: *ASTM Designation C1161-80—Standard Test Method for Flexural Strength of Advanced Ceramics at Ambient Temperature*, ASTM, Philadelphia, PA.
15. J. Dubsky, B. Kolman, and M. Vysohlid: *United Thermal Spray Conf.*, E. Lugscheider and P. A. Kammer, eds., Verlag fur Schweissen und verwandte Verfahren DVS-Verlag GmbH, Dusseldorf, 1999, pp. 659-63.